CHAPTER 4

Results and Discussions

In Chapter 3, principles, methods and procedures of electron beam property measurements are described. The considered properties are a bunch charge, an energy and a transverse beam emittance. In this chapter, results of all measurements are presented and discussed. Certain experimental conditions were performed for the measurement of each property. At the measurement locations, the electron beam properties can be different from the properties at the RF-gun exit because some properties, e.g. beam size and beam emittance, change when the beam travels through the accerator. Beam dynamics simulations were performed by setting initial conditions to be the same as in the experiments in order to compare the beam properties between simulation and measurement results.

4.1 Measurements of Electron Bunch Charge

In this study, the Faraday cup was used to measure the dark current and the electron bunch charge produced from the RF-gun. As mentioned in Chapter 3 that the electron micro-bunch charge can be measured with the Faraday cup because a spacing in time domain of each microbunch is long enough to measure with an oscilloscope due to the laser injection rate of 89.25 MHz. Prior to any bunch charge measurement, a background dark current was measured in order to be subtracted from the measured bunch charge value. An amount of the dark current depends on the RF power and the solenoid magnetic field. In the dark current measurement for each RF power, the solenoid magnetic field was varied to find an optimum value. An example result of the dark current measurement as a function of the solenoid magnetic field for the RF power of 8.9 MW with the RF macropulse duration of 2 μs is shown in Fig. 4.1. The result shows that the maximum charge of the dark current is 70 pC at the solenoid magnetic field of 178 mT. Dependences of the dark current and the optimal solenoid current on the RF power are shown in Fig 4.2. The charge of the dark current is proportional to the RF power, which is directly related to the electric field strength of the RF wave in the RF-gun, since the electric field is proportional to the square root of the RF power.

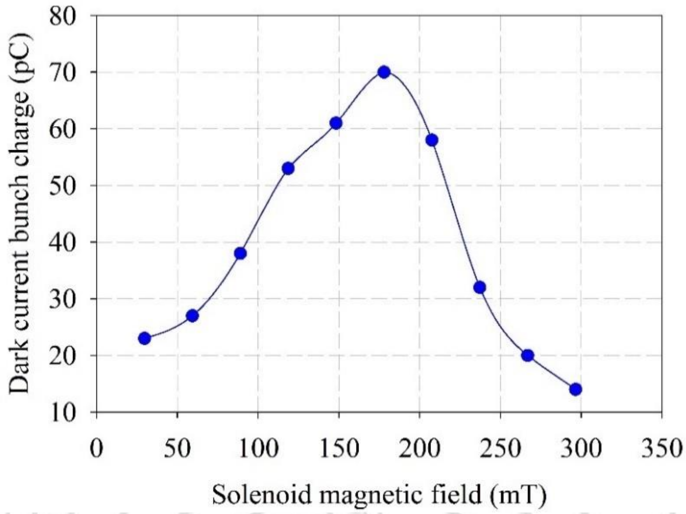

Figure 4.1: Charge of the dark current as a function of the solenoid magnetic field when the RF power of 8.9 MW was used.

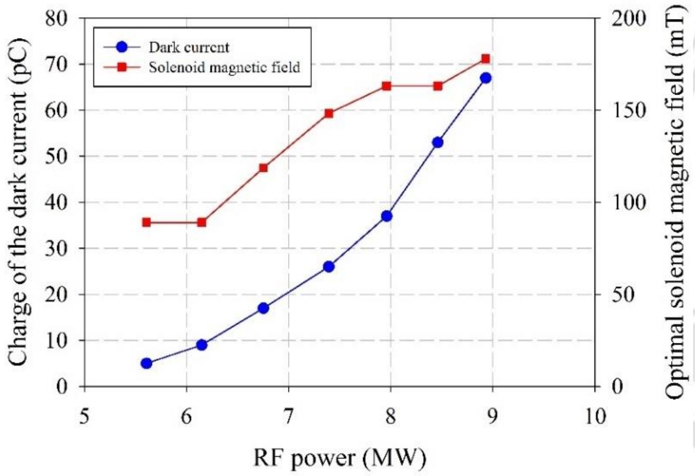

Figure 4.2: Charge of the dark current and the optimal solenoid magnetic field as a function of the RF power.

In the measurements of the electron bunch charge, an RF power of 8.9 MW and a solenoid magnetic field of 193 mT were used. The laser injection phase refers to the laser injection time, which is synchronized with the evolution time of the RF wave [48]. Since the magnitude of the electric field on the cathode surface is related to the laser injection phase, the amount of electron bunch charge is also related to the laser injection phase. In this study, the zero-crossing phase is defined as the phase without the emitted electron from the RF-gun. As described in the Chapter 2, the number of the emitted electron from the cathode depends on the excess energy $(h\nu - \phi)$ by the quadratic relation. The work function of the cathode material (ϕ) decrease when the external electric field is applied as shown in Eq. (2.29). The relationship between the electron bunch charge and the laser injection phase for different laser pulse energies are shown in Fig. 4.3.

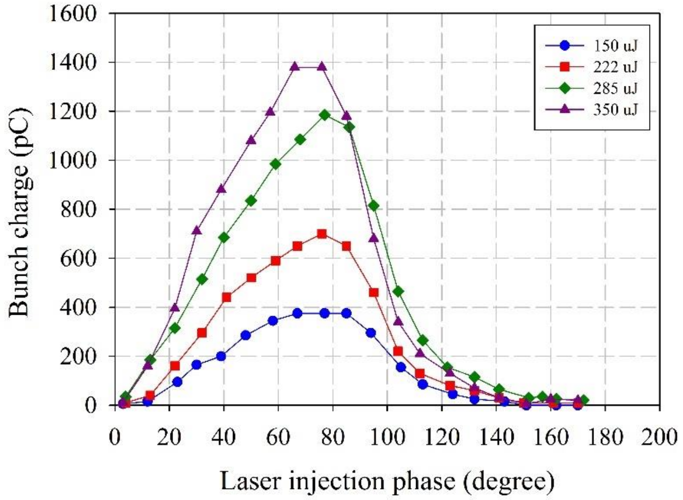

Figure 4.3: Dependence of the electron bunch charge on the laser injection phase when the drive laser pulse energies were 150, 222, 285 and 350 μJ. The solenoid magnetic field in these measurements was 193 mT.

The measurement results in Fig. 4.3 show that the electrons are generated and accelerated in the laser injection phase range of around 0-140 degree. At the phases lower than 65 degree, the bunch charge increased when the laser pulse increased and it dropped when the phases were larger than this value. At a certain phase, the bunch charge value was not linearly increased when the laser energy was large, as shown in Fig. 4.4.

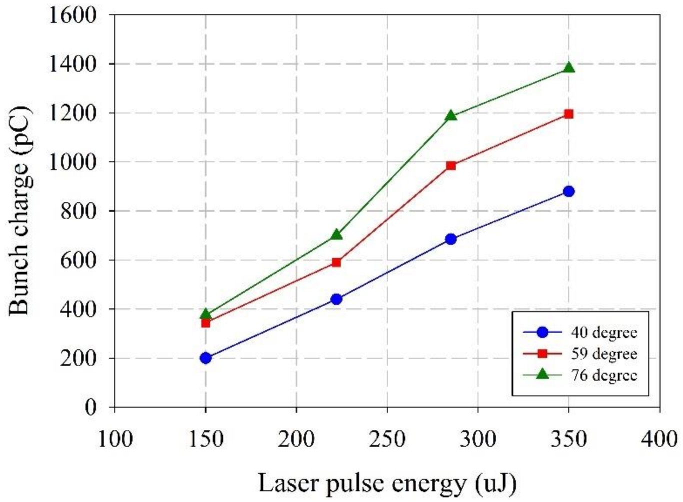

Figure 4.4: Relationship between the electron bunch charge and the drive laser pulse energy when the laser injection phases were 40, 59 and 76 degree.

At the laser injection phase of 40 degree, the number of generated electron linearly increased when the leser pulse energy increased. The results show the difference for the phase of 59 and 76 degree, the number of generated electron is large at high laser pulse energy while the stored energy inside the RF-gun, which is used for electron acceleration, is limited by the electric field of the RF wave. The energy gain of each electron is small because the stored energy is distributed among a large number of electrons. The space charge effect is high when the energy is low. This leads to large divergence beam for low energy electrons. Then, some electrons exit from the RF-gun but some electrons have large divergence and hit the wall of the gun. Therefore, the bunch charge does not linearly increase as a function of the laser pulse energy when the laser injection phase is large.

4.2 Measurements of Electron Beam Energy

Measurements of electron beam energy were performed by using a dipole magnet and a fluorescent screen equipped with a CCD camera as described in Chapter 3. The dipole magnet is installed downstream the beam extraction window where the center position of the 3-D field distribution of the dipole magnet is at z = 154.75 cm, while the center of the fluorescence screen is then located at z = 168 cm and x = - 6 cm. In order to measure an averge beam energy, the electron beam image was brought to the center of the screen by adjusting the dipole magnet current. A trajectory of an electron with no angular displacement is used as a guideline to determine the electron energy when it travels through the magnetic field of the dipole magnet. In this calculation, 3-D magnetic field distribution obtained from the measurements wass included in PARMELA simulation.

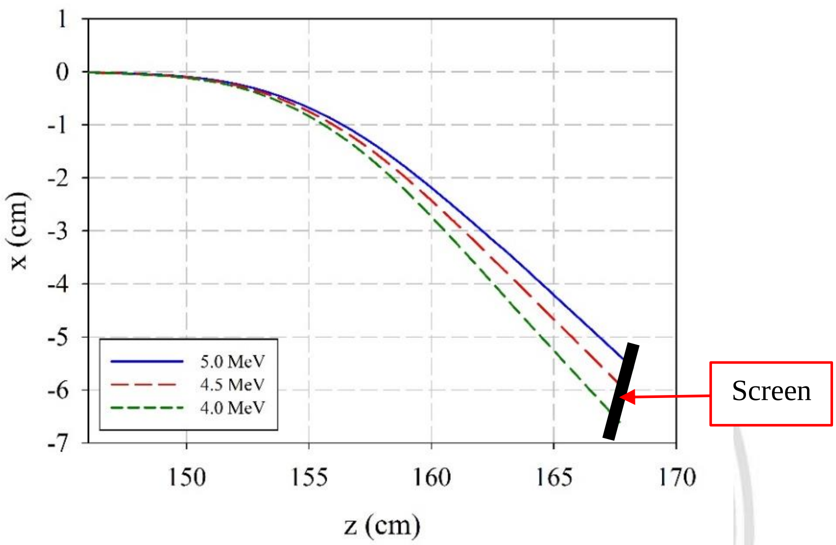

Figure 4.5: Trajectories of electrons with the energies of 5, 4.5 and 4 MeV along the 3-D dipole magnetic field distribution when the applied current is 4.25 A. The fluorescence screen center is at the z-position of 168 cm.

Examples of electron trajectories for electrons with three different energies; 4.0, 4.5 and 5.0 MeV, when using the dipole magnet current of 4.25 A are shown in Fig.4.5. The electrons with the energies of 4.0 and 5.0 MeV incident on the screen with different positions on the x-axis of 11.9 mm. This results in the calibration value of the electron energy and the x-position on the screen of 80 keV/mm. In this study, the horizontal width of the screen is 30 mm. Thus, the electron, which enters the dipole magnetic field with no angular displacement and incidents on the edges of the screen (±15 mm), has the energy of ±1.2 MeV from the mean energy. For example, the electron with energy (E) of 4.5 MeV incidents on the screen center. The electrons, which incident on both edges of the screen have the energy different (ΔE) of 2.4 MeV. Thus, this energy spectrometer has the minimum resolution ($E/\Delta E$) of 1.875.

Practically, the actual electron beam has a certain beam size and some angular displacement. It may enter the dipole magnetic field with diverging or converging angles. Then, the electrons with different energies have a possibility to incident on the screen with the same position. On the other hand, the electrons with the same energy have a possibility to incident on the screen on the different positions. This leads to the difficulty on determining the actual electron beam energy when the beam is observed on the screen. An example of the measured electron beam intensity distribution on the x-axis of the screen is shown in Fig. 4.6.

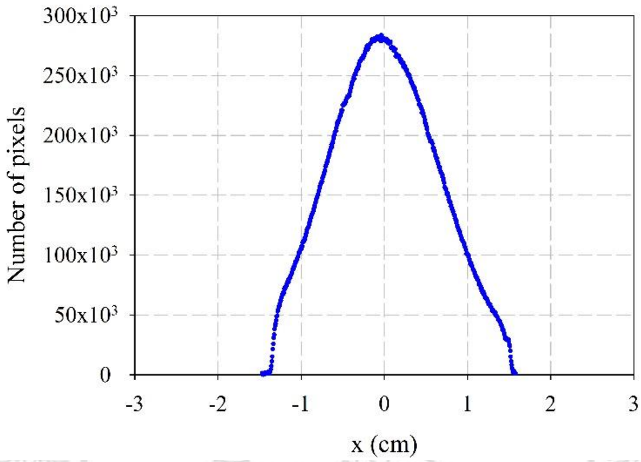

Figure 4.6: Measured electron beam intensity distribution on the x-axis of the screen when the RF power was 8.9 MW, the laser injection phase of 40 degree and the solenoid magnetic field of 200 mT were used.

The measurement result shows that the electrons with various energies incident on the screen with wide area. In this measurement, the dipole magnet current of 4.36 A was used to bring the peak of the electron distribution, which represents the maximum number of electrons, to be at the screen center. Thus, the mean energy of the electron beam is 4.6 MeV. If consider the energy spread of this beam image on the screen, it would result in the energy spread of ±1.2 MeV. However, this value is seemed to be too large for the actual energy spread of the electron beam produced from the photocathode RF-gun with maximum acceleration. This can be explained that the electron beam scatters when it hits on the beam extraction window and travels in the air. The beam size on the screen is large due to these scatterings.

Beam dynamic simulations with the same accelerator conditions as in the measurement cases were performed by using the program PARMELA. The simulated parameters used in all simulations in this thesis are listed in Table 4.1. The photocathode of the RF-gun in the simulations is flat and has a diameter of 0.6 cm. It is located at the position z = 0 cm. Photoelectrons perpendicularly emit from the cathode surface with an initial energy of 10 eV. The initial energy spread at the cathode surface is zero. The simulated electron radial distribution is the Gaussian distribution with a characteristic width, which is defined by the laser spot size of 1.378 mm at FWHM. The RF phase difference between the half-cell and the full-cell cavities is 180 degree because this RF-gun accelerates the electrons in the π-mode. The RF-gun accelerating gradient of 52 MV/m and the laser injection phase of 40 degree were used. These conditions correspond to the electron beam energy of 4.6 MeV at the RF-gun exit. The solenoid magnetic fields of 150 and 200 mT were used in the simulations. Examples of simulated electron distributions on the x-axis of the screen when using the simulation conditions as mentioned above and the dipole magnet current of 4.36 A are shown in Fig. 4.7.

Table 4.1: Measured and simulated parameters used in the study of beam energy measurements.

Parameter	Measurement	Simulation
Resonant frequency of RF-gun	2,856 MHz	2,856 MHz
Laser spot size at FWHM	1.378 mm	1.378 mm
Laser pulse length at FWHM	≈ 8 ps	8 ps
Initial energy at cathode	NA	10 eV
Electron bunch charge	50 pC	50 pC
Laser pulse energy	180 μJ	NA

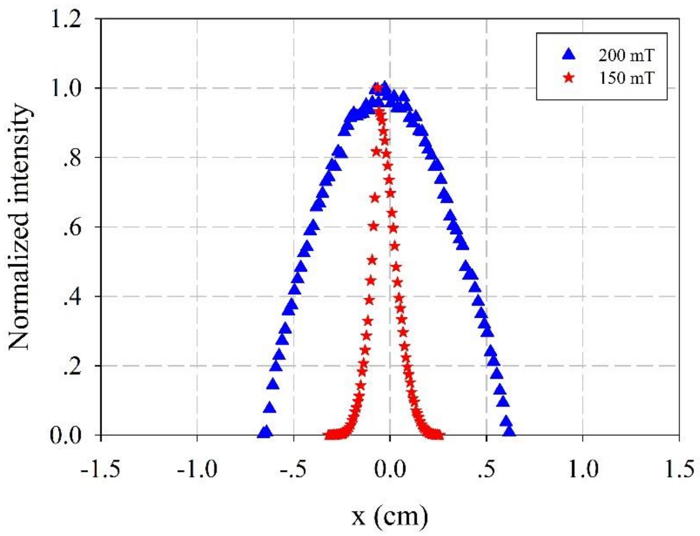

Figure 4.7: Simulated electron distributions on the x-axis of the screen when the RF-gun accelerating gradient of 52 MV/m, the laser injection phase of 40 degree and the solenoid magnetic fields of 150 and 200 mT were used.

Both simulation results provide smaller energy spread values than the case of the measurement. The reason can be that in the measurement the beam may scatter when the beam hits the extraction window and travels in the air. This would lead in a wider beam size and larger divergence before it enters the dipole magnetic field. The wider transverse beam size and larger divergence at the entrance of the dipole magnet would result in broader beam distribution on the screen in the dispersive section. Therefore, the measured energy spread value obtained from the measurement with this setup may not be the actual value of the beam.

The electron beam energy depends greatly on the accelerating gradient in the resonant cavities, which is related directly to the power of the RF wave and the laser injection phase. The measurements of the electron beam energy for different RF powers and laser injection phases were performed. During the measurements, the laser pulse energy of 180 µJ was used and the dipole magnet current was adjusted to keep the incident beam on the screen center for each RF power and laser injection phase. The energy gain of the emitted electron depends on the electric field magnitude and the number of electrons. The electrons are generated over the laser pulse duration of around 8 ps, which corresponds to 8.22 degree for the RF frequency of 2856 MHz. The measurement results in Fig. 4.8 show that the beam mean energy values are almost constant when the laser injection phase is in the range of 10-50 degree. The increasing rate of the emitted electrons and the accelerating gradient are seemd to be balance in this phase range. At the phases of larger than 60 degree, the beam energy decreases because the number of emitted electrons on the cathode surface is large (in order of 400 pC). Thus, the energy gain of the electron is small when the laser injection phase is large

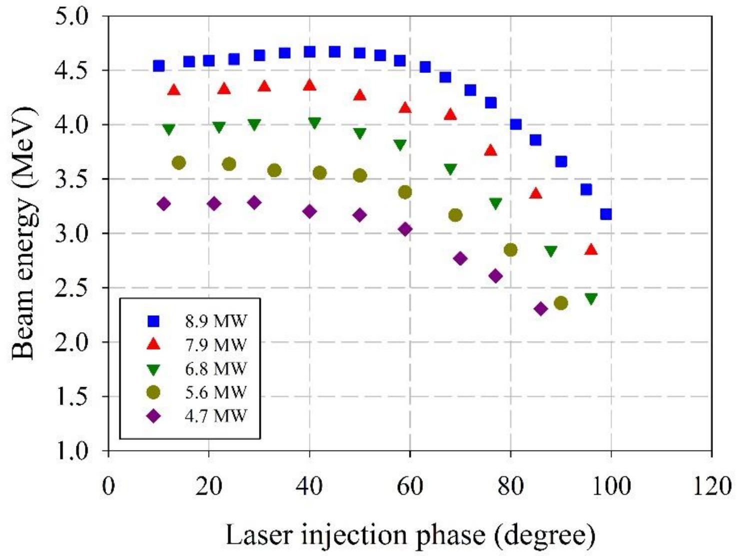

Figure 4.8: Measurement results of the electron beam energy for various RF powers and laser injection phases for different accelerating gradients E_1 and E_2.

The beam dynamic simulation with the simulated parameters listed in Table 4.1 was conducted to estimate the beam energy for each RF power and laser injection phase. The simulation result for energy optimization reveals that the accelerating gradients in the half-cell and the full-cell cavities, which provide the beam energy of 4.6 MeV, are 52 MV/m [49]. Comparison between the measurement and simulation results of the beam energy dependence on the laser injection phase for the maximum mean beam energy of about 4.6 MeV is shown in Fig. 4.9. The blue solid circle plots are the measurement results and the red solid rectangual plots are the simulation results.

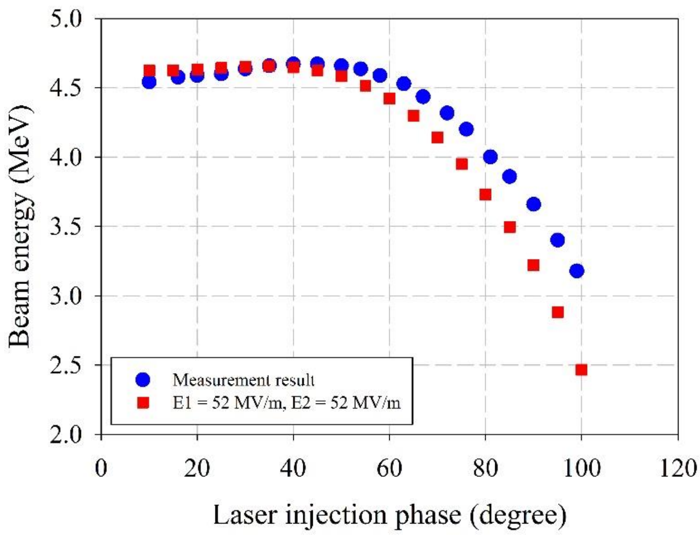

Figure 4.9: Measurement and simulation results of the beam energy dependence on the laser injection phase for the case of the maximum mean beam energy of about 4.6 MeV.

The measured results as shown in Fig. 4.9, the beam energy is maximum at the laser injection phase of 40 degree. In case of the simulated results, the beam energy is maximum at the laser injection phase of around 35-40 degree. Moreover, the simulations were performed to find the accelerating gradients that correspond to the measured RF powers of 8.9, 7.9, 6.8, 5.6 and 4.7 MW. The study results show that the RF-gun operation with the accelerating gradients of 52, 49, 44.5, 40 and 37 MV/m produces electron beams with the same maximum energies, which are obtained from the RF powers of 8.9, 7.9, 6.8, 5.6 and 4.7 MW, respectively. The results from these simulations are shown in Fig. 4.10, which the solid and the hollow plots refer to the beam energy and the energy spread, respectively. It is noted that the design mean beam energy for the KU photocathode RF-gun is 5 MeV, which requires the accelerating gradient of 55 MV/m. However, the measurement results reveal that the measured maximum beam energy is about 4.5-4.6 MeV, which corresponds to the accelerating gradient of 50-52 MV/m.

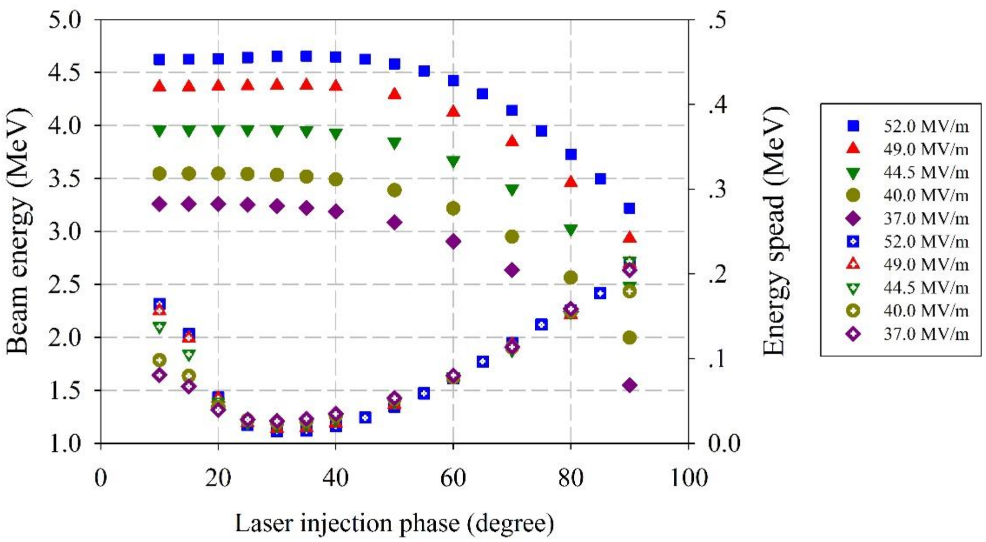

Figure 4.10: Simulated electron beam energy and energy spread as a function of the laser injection phase for different accelerating gradients E_1 and E_2.

4.3 Measurements of Beam Transverse Emittance

The transverse beam emittance is strongly related to electron beam energy and bunch charge as well as internal and external electromagnetic forces. Therefore, the emittance measurement is important for selecting an appropriate RF power, laser injection phase and solenoid magnetic field. The measurement system is prepared in form of the quadrupole scan method with a thin lens approximation as described in Chapter 3. The emittance measurements were performed in-vacuum condition. This section presents the experimental results of the beam emittance dependence on the electron bunch charge, the solenoid magnetic field and the RF phase. All transverse beam emittance measurements presented in this thesis were performed with the quadrupole magnet at the position of 112 cm from the cathode surface or equivalent to 100 cm downstream the RF-gun exit.

Beam dynamic simulations with PARMELA program were performed to compare the results with the measured emittance values. The beam emittance value achieved from the simulation is the RMS beam emittance, which is directly calculated from the transverse and the angular displacements of the macroparticles. Some examples of the simulated RMS beam emittance values, which are achieved by using the quadrupole scan method are presented to compare with the results from the measurements and from the direct statistical calculation.

4.3.1 Beam Emittance and Solenoid Magnetic Field

The solenoid magnet is installed at the RF-gun exit with the magnetic field distribution that also occupies some space inside the RF-gun. It is used to focus the electron beam during and after the acceleration. The force due to the solenoid magnetic field changes a focusing condition of the beam along the z-axis and also changes an angular displacement of electrons inside the electron beam. Therefore, it is important to study the dependence of the beam transverse size and emittance on the solenoid magnetic field. In this study, an RF power of 9 MW and the laser injection phase of 40 degree were used to accelerate an electron beam with a bunch charge of 50 pC. With these conditions, the electron beam exits the RF-gun with the energy of around 4.6 MeV. It was experimentally found that electrons can not be formed to be an electron beam if there is no focusing from the solenoid magnrtic field. Electron beams can be formed with the solenoid magnetic fields of 170-230 mT. Relationships between the horizontal and vertical RMS beam size squared and the quadrupole magnet focal length used in the quadrupole scan measurements are shown in Fig. 4.11 and Fig. 4.12.

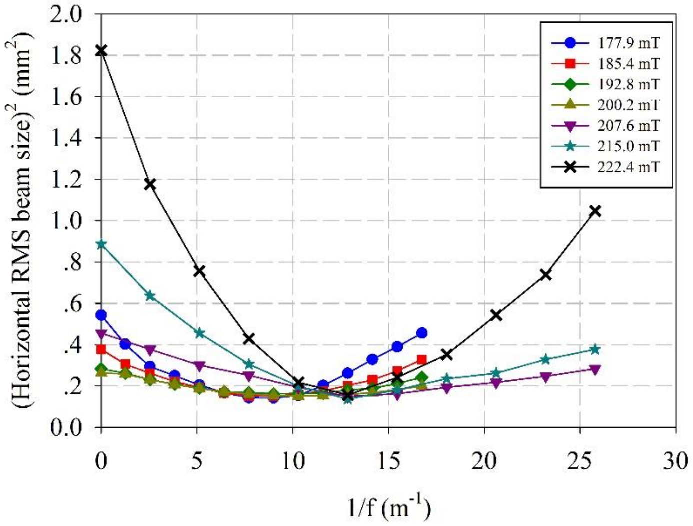

Figure 4.11: Measured horizontal RMS beam size squared as a function of the quadrupole magnet focal length for various solenoid magnetic fields.

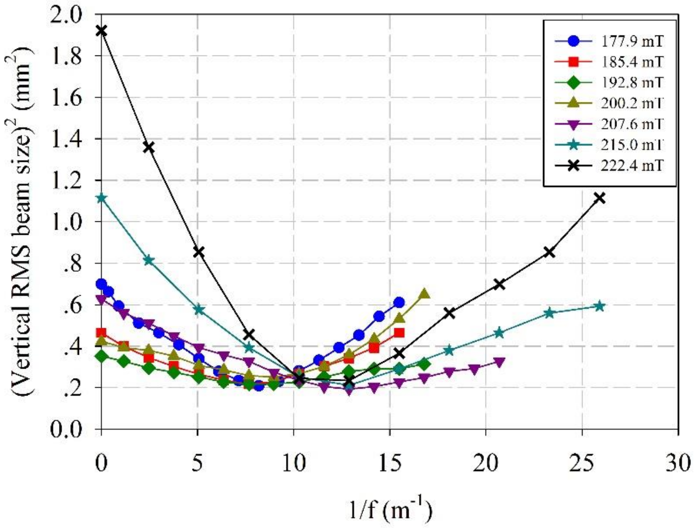

Figure 4.12: Measured vertical RMS beam size squared as a function of the quadrupole magnet focal length for various solenoid magnetic fields.

As shown in both figures, for the solenoid magnetic fields of 177.9 – 200.2 mT the smallest beam size of around 0.52 mm was obtained when the quadrupole magnet gradient was 2.5 T/m, which corresponds to the quadrupole focal length of around 11.2 cm. In case of the solenoid magnetic fields of larger than 200.2 mT, the smallest beam size of around 0.44 mm was measured when the quadrupole magnet gradient was 3.6 T/m, which correspond to the quadrupole focal length of around 7.6 cm. The quadrupole magnetic focusing conditions are difference for different solenoid magnetic field ranges because the solenoid magnetic field forms the beam with different initial conditions. An example of the relationship between the vertical RMS beam size squared and the quadrupole magnet focal length when using the solenoid magnetic field of 177.9 mT is obtained from the following equation

$$\sigma^2 = 6.9357\times10^{-9}\frac{1}{f^2} - 1.1268\times10^{-7}\frac{1}{f} + 7.0827\times10^{-7}, \qquad (4.1)$$

where σ is the RMS beam size on the fluorescence screen and f is the focal length of the quadrupole magnet. The R squared value of the fitting in the Eq. (4.1) is 0.9804. The matrix element $(\sigma_s)_{11}$ is obtained from equation (2.128)

$$((\sigma_s)_{11})^2 = D^2(\sigma_q)_{11}\frac{1}{f^2} - 2D\left\{(\sigma_q)_{11} + D(\sigma_q)_{12}\right\}\frac{1}{f} + \left\{(\sigma_q)_{11} + 2D(\sigma_q)_{12} + D^2(\sigma_q)_{22}\right\},$$

where $(\sigma_s)_{11}$ is the RMS beam size on the fluorescense screen and D is the distance from the quadrupole magnet center to the screen center, which is 14 cm. Therefore, the matrix elements $(\sigma_q)_{11}$, $(\sigma_q)_{12}$, $(\sigma_q)_{21}$ and $(\sigma_q)_{22}$ at the quadrupole magnet can be calculated and the results are

$$(\sigma_q)_{11} = \frac{6.9357\times10^{-9}}{D^2} = \frac{6.9357\times10^{-9}}{(14\times10^{-2})^2} = 3.539\times10^{-7}\,m^2,$$

$$(\sigma_q)_{12} = (\sigma_q)_{21} = \frac{1}{D}\left(-\frac{1.1268\times10^{-7}}{2D} - (\sigma_q)_{11}\right) = 3.469\times10^{-7}\,m,$$

$$(\sigma_q)_{22} = \frac{\left(7.0827\times10^{-7} - (\sigma_q)_{11} - 2D(\sigma_q)_{12}\right)}{D^2} = 1.313\times10^{-5}\,m^{-1}rad.$$

The RMS emittance is a square root of a determinant of the beam matrix at the quadrupole magnet, which is

$$\varepsilon_{RMS} == \sqrt{\{(\sigma_q)_{11}\times(\sigma_q)_{22}\} - \{(\sigma_q)_{12}\}^2} = 2.127\times10^{-6} = 2.127\ mm-mrad..$$

For electrons with the beam energy of 4.67 MeV, the Lorentz factor γ and the velocity β are calculated to be 10.1409 and 0.99399, respectively. Therefore, the normalize emittance is calculated to be

$$\varepsilon_n = \gamma\beta\varepsilon_{RMS} = 10.1409\times0.99399\times2.127 = 21.44\,mm-mrad.$$

The beam emittance values for other solenoid magnetic fields were obtained by using the same procedure. The measured RMS transverse beam size and beam emittance as a function of the solenoid magnetic field are shown in Fig. 4.13 and 4.14, respectively. Red and blue plots in this figure refer to a property in x-axis and y-axis, respectively.

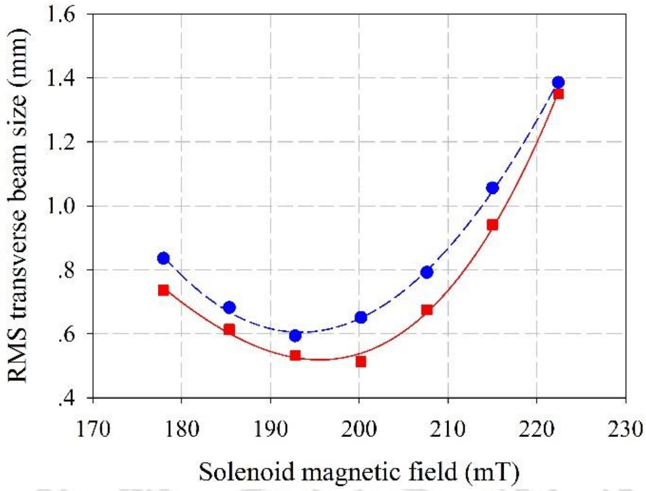

Figure 4.13: Relationship between the measured RMS transverse beam size and the solenoid magnetic field. Red and blue plots in this figure refer to a property in x-axis and y-axis, respectively.

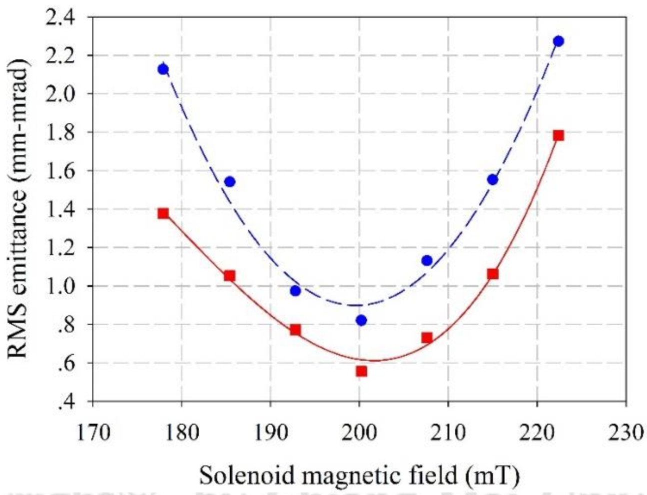

Figure 4.14: Relationship between the measured RMS beam emittance and the solenoid magnetic field. Red and blue plots in this figure refer to a property in x-axis and y-axis, respectively.

The fitting of the RMS transverse beam size as a function of the solenoid magnetic field in the x-axis (red solid line) and y-axis (blue dash line) are obtained from equations (4.2) and (4.3), respectively. The R squared values of the fitting for the x-axis and y-axis are 0.9978 and 0.9989, respectively.

$$\sigma_{RMS,x} = 9.774\times10^{-6}B^3 - 4.8\times10^{-3}B^2 + 7.71\times10^{-1}B - 38.316 \qquad (4.2)$$

$$\sigma_{RMS,y} = -1.501\times10^{-6}B^3 + 1.8\times10^{-3}B^2 - 5.447\times10^{-1}B + 47.846 \qquad (4.3)$$

The fitting of the RMS beam emittance as a function of the solenoid magnetic field in the x-axis (red solid line) and y-axis (blue dash line) are obtained from the equation (4.4) and (4.5), respectively. The R squared values of the fitting for the x-axis and y-axis are 0.9945 and 0.9868, respectively.

$$\varepsilon_{RMS,x} = 3.039\times10^{-5}B^3 - 1.63\times10^{-2}B^2 + 2.861B - 163.267 \qquad (4.4)$$

$$\varepsilon_{RMS,y} = -6.167\times10^{-7}B^3 + 3.1\times10^{-3}B^2 - 1.145B + 112.732 \qquad (4.5)$$

The experimental results in Fig. 4.13 and Fig. 4.14 show that the minimum beam emittance value of around 0.6 - 0.8 mm-mrad was measured with the solenoid magnet field of 200 mT. The minimum emittance values in x-axis and y-axis have the difference of about 33% at the solenoid magnetic field of 200 mT. The minimum RMS transverse beam size in the x-axis is 0.51 mm when the solenoid magnetic field is 200 mT, while the minimum RMS transverse size in the y-axis is 0.59 mm when the solenoid magnetic field is 193 mT.

The parameters used in simulations for emittance measurement are the same as in Table 4.1, except the solenoid magnetic fields of 100 - 230 mT were used. The bunch charge was fixed at 50 pC. For all simulations in this section, the accelerating gradient was set to 52 MV/m and the laser injection phase was kept at 35 degree in order to obtain the maximum beam energy equal to the measured value. The RMS transverse beam size at the screen position (z = 126 cm) and the RMS emittance at the quadrupole magnet (z = 112 cm) are calculated to compare with the measured results. Dependences of the RMS transverse beam size and the beam emittance on the solenoid magnetic field and the laser injection phase are shown in Fig. 4.15 and 4.15, respectively.

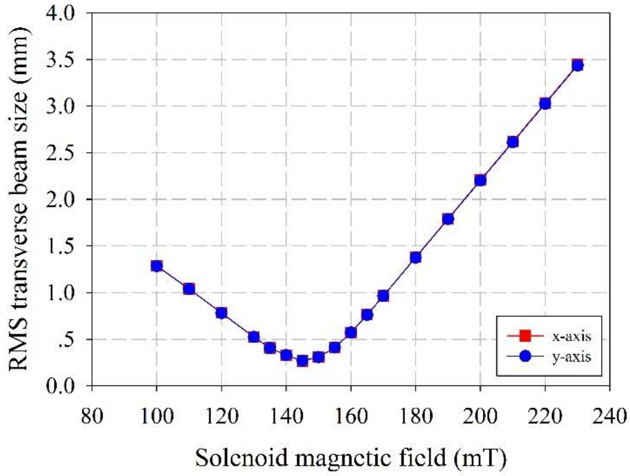

Figure 4.15: Simulated RMS transverse beam size dependence on the solenoid magnetic field at the position z = 126 cm.

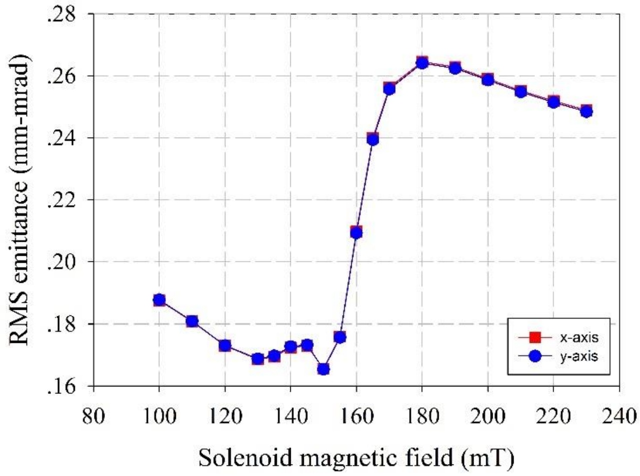

Figure 4.16: Simulated RMS emittance as a function of the solenoid magnetic field at the position z = 112 cm.

The simulation results show that the minimum RMS transverse beam size is 0.3 mm when the solenoid field is 150 mT. The minimum RMS emittance is about 0.166 mm-mrad when using the solenoid field of 150 mT. For the solenoid magnetic field of 200 mT, which is the optimal value in the measurement, the RMS transverse beam size is 2.2 mm and the RMS emittance is 0.26 mm-mrad. The differents in the optimal values of solenoid magnetic fields and the difference for simulation and measurement may be due to the different of the off-axis magnetic field distributions and other causes, which are suggested later in section 4.4.

4.3.2 Beam Emittance and Electron Bunch Charge

An electron bunch is a group of moving electrons. Therefore, the repulsing force between electron and the space charge effect are related to a number of electrons inside the bunch. The more bunch charge, the more repulsion force and the space-charge effect. Both the repulsing force and the space charge effect affect significantly on the transverse beam emittance. In this measurement, an RF power of 8.9 MW, a laser injection phase of 40 degree and a solenoid magnetic field of 193 mT were used to study the beam emittance dependence on the bunch charge and the drive laser pulse energy. This condition corresponds to the electron beam energy of around 4.6 MeV. The relationship between the measured RMS transverse beam size squared and the quadrupole magnet focal length (f) is shown in Fig. 4.17.

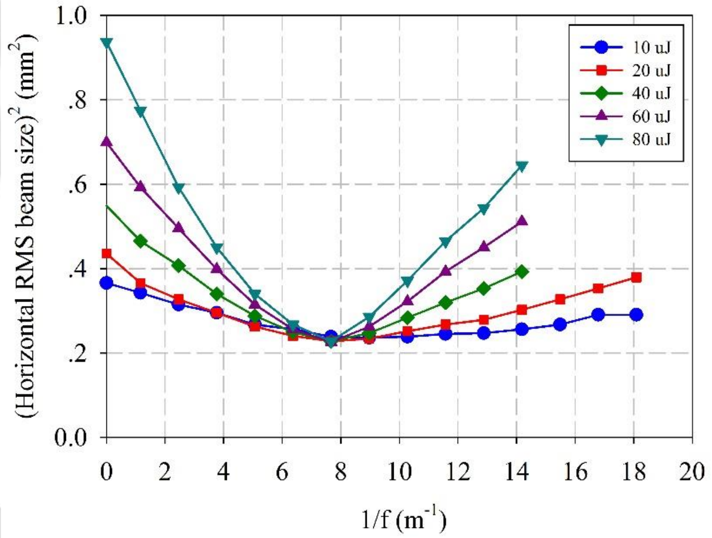

Figure 4.17: RMS transverse beam size dependence on the quadrupole magnet focal length for the drive laser pulse energy of 10, 20, 40, 60 and 80 µJ.

As shown in Fig. 4.17 that without the quadrupole focusing, the transverse beam sizes are proportional to the laser pulse energy, which has linear relationship with the electron bunch charge at the laser injection phase of 40 degree. For all bunch charges, the smallest beam size of around 0.47 mm was measured when a quadrupole magnet gradient is 2.16 T/m. This is correlated to the quadrupole magnet focal length of around 7.67 m^{-1}. As an example, the relationship between the RMS beam size square (σ^2) and the quadrupole magnet focal length (f) when using the drive laser pulse energy of 10 μJ is obtained from

$$\sigma^2 = 1.1498 \times 10^{-9} \frac{1}{f^2} - 2.4313 \times 10^{-8} \frac{1}{f} + 3.663 \times 10^{-7}, \qquad (4.6)$$

The R squared value of the fitting in Eq. (4.6) is 0.9799. Comparing the coefficients in equation (4.6) with the transport matrix element as described in Chapter 2, the elements $(\sigma_q)_{11}$, $(\sigma_q)_{12}$, $(\sigma_q)_{21}$ and $(\sigma_q)_{22}$ at the entrance of the quadrupole magnet can be calculated to be

$$(\sigma_q)_{11} = \frac{1.1498 \times 10^{-9}}{D^2} = \frac{1.1498 \times 10^{-9}}{(14 \times 10^{-2})^2} = 5.866 \times 10^{-8}\, m^2,$$

$$(\sigma_q)_{12} = (\sigma_q)_{21} = \frac{1}{D}\left(-\frac{2.4313 \times 10^{-8}}{2D} - (\sigma_q)_{11} \right) = 2.012 \times 10^{-7}\, m,$$

$$(\sigma_q)_{22} = \frac{\left(3.662 \times 10^{-7} - (\sigma_q)_{11} - 2D(\sigma_q)_{12}\right)}{D^2} = 1.2816 \times 10^{-5}\, m^{-1} rad.$$

Then, the RMS emittance at the quadrupole magnet is

$$\varepsilon_{RMS} = \sqrt{\{(\sigma_q)_{11} \times (\sigma_q)_{22}\} - \{(\sigma_q)_{12}\}^2} = 0.8434\, mm - mrad.$$

For the beam energy of 4.67 MeV, the Lorentz factor γ and the velocity β are calculated to be 10.1409 and 0.99399, respectively. The normalize emittance becomes

$$\varepsilon_n = \gamma\beta\varepsilon_{RMS} = 8.50\, mm - mrad.$$

The beam emittance values for other drive laser pulse energies can be calculated by using the same procedure. Retionships between the RMS transverse beam sizes at the screen and beam emittance values at the quadrupole magnet for varions electron bunch charges are shown in Fig. 4.18. Red square plots and blue circle plots are the RMS transverse beam size and the RMS emittance, respectively.

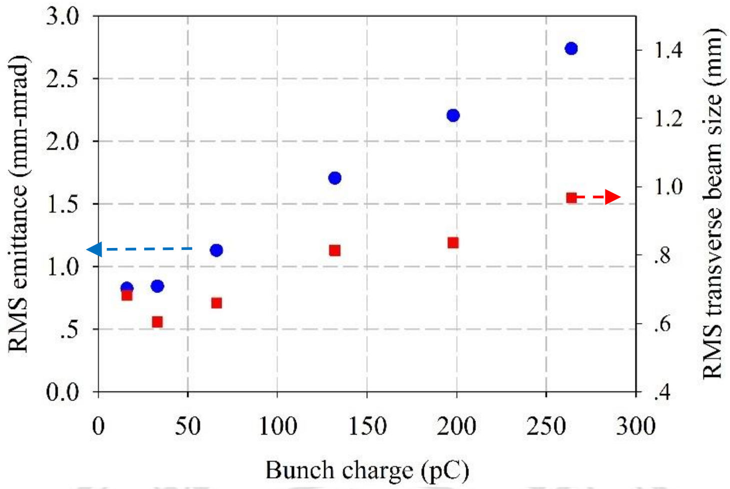

Figure 4.18: Measured RMS transverse beam size at the screen (red square plots) and the measured RMS emittance (blue circle plots) at the quadrupole magnet as a function of the electron bunch charge when the solenoid magnetic field is 193 mT.

The simulations parameters are the same as in Table 4.1, except the electron bunch charge was varied. Two solenoid magnetic field values of 150 and 193 mT were used. The accelerating gradient was kept at 52 MV/m and the laser injection phase was set to 35 degree to obtain the maximum energy as same as the measurement studies. Then, the electron beam properties at the experimental station (z = 112 cm) were studied by using the bunch charges in the range of 10-300 pC. The RMS transverse beam size and the RMS emittance dependence on the bunch charge and the RF phase are shown in Fig. 4.19 and 4.20, respectively. For the solenoid magnetic field of 193 mT, the simulation show the difference tendency compared with the measurement results. When the solenoid magnetic field of 150 mT is used, tendencies of the RMS transverse beam size and the beam emittance as a function of the bunch charge are more similar to the measurement results than the case of the solenoid magnetic fiel of 193 mT. This can be explained that the integrated magnetic field along the z-axis of the actual solenoid magnet may be different from the simulated one.

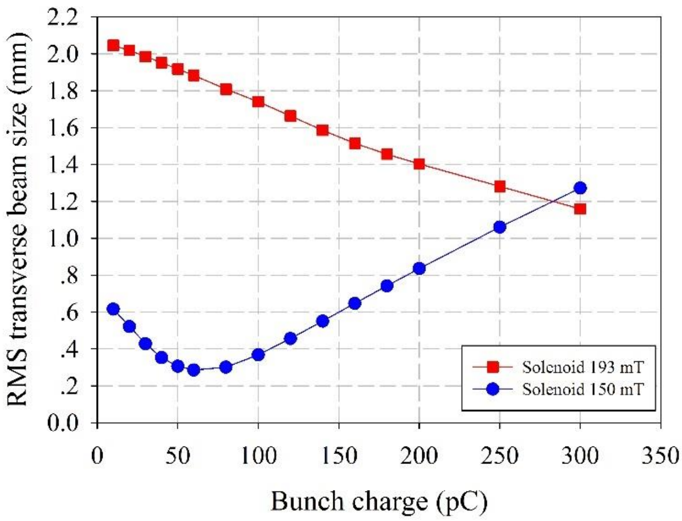

Figure 4.19: Simulated RMS transverse beam size dependence on the bunch charge and the solenoid magnetic field at the position z = 126 cm.

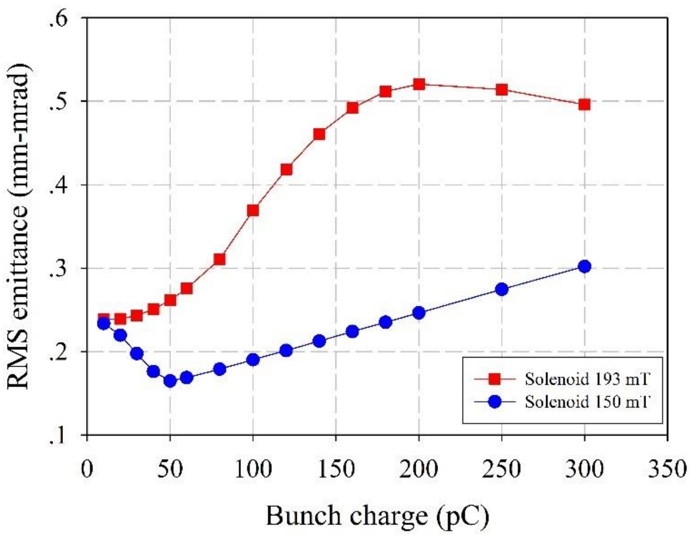

Figure 4.20: Simulated RMS emittance dependence on the bunch charge and the solenoid magnetic field at the position z = 112 cm.

Electron bunches are focused by the magnetic field component of the RF wave and the solenoid magnetic field while they are accelerated through the RF-gun. The influence of the focusing changes the RMS transverse size and emittance of electron beams. The measurement results in Fig. 4.18 show that the bunch charge and the transverse beam emittance are almost linearly proportional to the laser pulse energies when the bunch charge is larger than 30 pC. It is noted that the repulsing force and the space charge effect, which are larger for the higher bunch charges, make the electrons getting large transverse and angular displacements. Therefore, the beam emittance is getting larger for higher laser pulse energy.

4.3.3 Beam Emittance and Laser Injection Phase

A magnitude of the electric field changes with time when the electrons are accelerated through the RF-gun. Thus, the electron beam energy as well as the beam emittance depend on the accelerating gradient and the laser injection phase. Since the number of emitted electrons from the cathode is related to the electric field on the cathode surface. In this study the laser intensity was adjusted to achieve a constant bunch charge for each laser injection phase. The RF power of 9 MW, the solenoid magnetic field of 200 mT and the bunch charge of 50 pC are used. The relationships between the horizontal RMS transverse beam size squared and the quadrupole magnet focal length for difference laser injection phase are shown in Fig. 4.21.

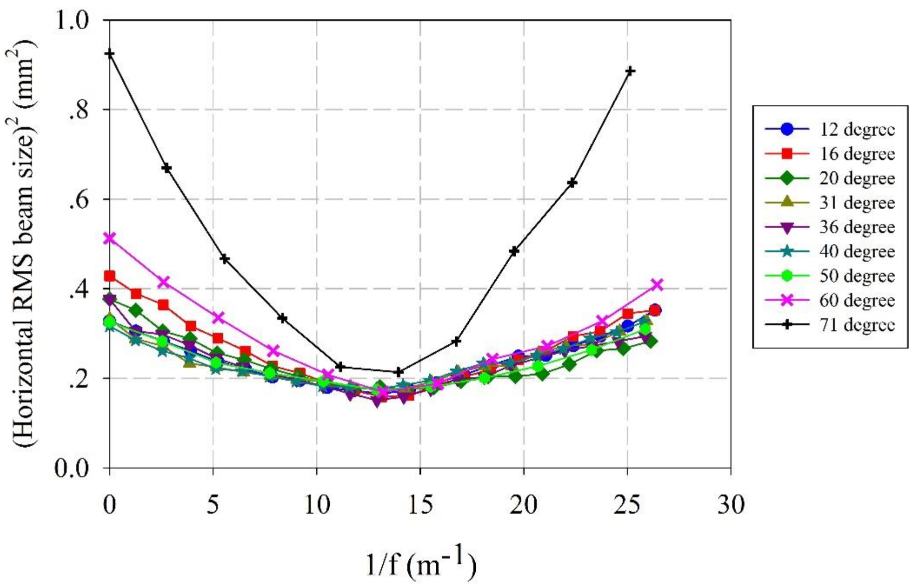

Figure 4.21: Measured horizontal RMS transverse beam size squared as a function of the quadrupole magnet focal length for different laser injection phases.

As shown in Fig. 4.21, the initial transverse beam sizes are proportional to the laser injection phase when the current of the quadrupole magnet Q_3 is zero. For all laser injection phases, the smallest beam size of around 0.44 mm was measured when the quadrupole magnet gradient is 3.6 T/m, which is related to the quadrupole magnet focal length of 7.63 cm. For the phases of 12-60 degree, the relationships between the RMS beam size squared and the value of 1/f show the same tendency. This is because the beam energies for these phases are not so much difference and the quadrupole focusing conditions are almost the same. The beam matrix elements $(\sigma_q)_{11}$, $(\sigma_q)_{12}$, $(\sigma_q)_{21}$ and $(\sigma_q)_{22}$ as well as the RMS emittance values were obtained by using the same procedure described in section 4.3.1 and 4.3.2.

For the simulations, the beam emittance dependence on the accelerating gradient and laser injection phase were studied by using the simulated parameters as listed in Table 4.1, except the laser injection phase and the solenoid magnetic field. In this section, the RMS emittance is calculated in two difference methods. For the first method, the RMS emittance is calculated from the electrons transverse displacement (*x* or *y*) and the angular displacement (x' or y'). The solenoid magnetic field of 150 and 200 mT were used. The second method, the beam emittance value is obtained by following the quadrupole scan method. For the quadrupole magnet gradients of 0-5 T/m and the solenoid magnetic field of 200 mT. The dependences of the RMS transverse beam size at the screen position and the RMS beam emittance on the laser injection phase are shown in Fig. 4.22, and Fig. 4.23, respectively. In both figures, the blue circle plots represent the measurement results, the red square plots represent the simulation results, which are calculated by using the quadrupole scan method with the solenoid magnetic field of 200 mT, the green triangle plots represent the simulation results, which are calculated directly from the electron distribution with the solenoid magnetic field of 200 mT and the yellow triangle plots represent the simulation results, which are calculated from the electron distribution with the solenoid magnetic field of 150 mT. It can be seen from Fig. 4.22 that the simulated RMS transverse sizes, which are calculated from the electron distribution with the solenoid magnetic field of 150 mT (yellow triangle plots) are in the same order of the measurement results for the injection phase of 10-40 degree.

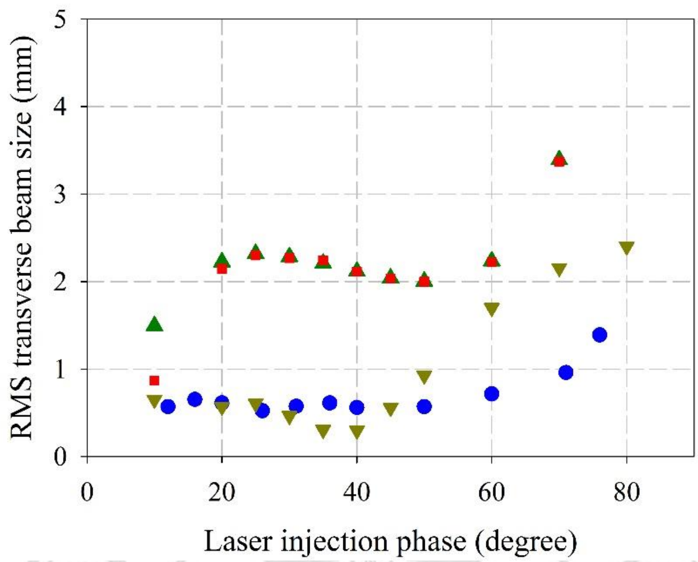

Figure 4.22: RMS transverse beam size at the screen position as a function of the laser injection phase.

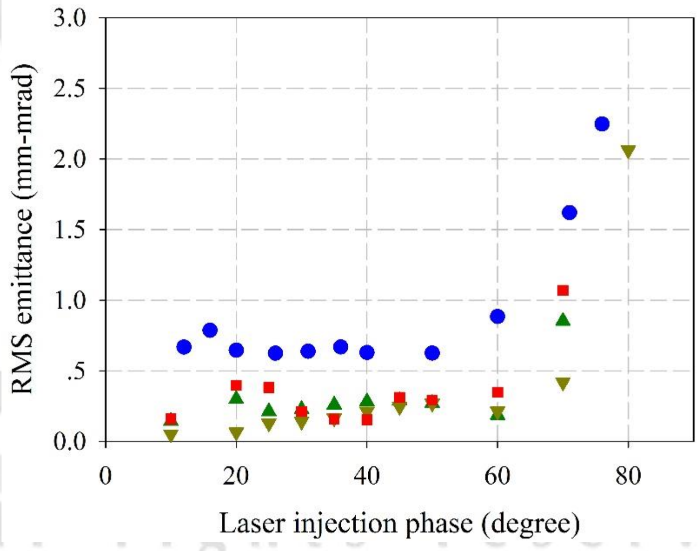

Figure 4.23: RMS transverse beam emittance at the quadrupole position as a function of the laser injection phase.

The measurement results in Fig. 4.23 show that the beam emittances are around 0.6-0.8 mm-mrad when the laser injection phases are lower than 50 degree. For this low phase region, the electrons are accelerated at the cathode surface when the electric field amplitude is high and the beam energies are high and almost constant around 4.5 - 4.7

MeV. Therefore, the beam emittances are low at this region. On the other hand, the beam energy rapidly decreases when the laser injection phases are higher than 50 degree, where the electrons are produced when the electric field is low and the space charge effect is high. Thus, the beam emittance rapidly increases in this region. The simulated beam emittance values obtained from all three methods are smaller than the measurement results.

4.4 Study on Influence of Laser Position on the Cathode

In this study, a fluorescense screen is used to observe the dark current and the electron beam transverse profile. The screen is located inside the vacuum chamber, which is installed downstream the laser port as shown in Fig. 3.26. The screen is located at the position z = 78 cm of the accelerator system. The dark current transverse profile depends on an amount of charge, an RF accelerating field and a solenoid magnetic focusing condition. In this study, the dark current was generated when the RF power of 8.9 MW was used. Some examples of dark current images on the screen for the solenoid magnetic fields of 0-297 mT are shown in Fig. 4.24. The intensity of the bright spot on the screen is proportional to the number of the incident electrons.

The dark current images show that the incident dark current diverges if without the solenoid magnetic focusing. The dark current beam is formed well when the solenoid magnetic field in the range of 118 - 200 mT is used. Then, the dark current diverses and vanishes when the solenoid magnetic field is larger than 222 mT. The center of the dark current beam does not change its position when the solenoid magnetic focusing changes. The dimensions of the screen and the image resolution of this setup are described in the Chapter 3.

When the electron beam is generated from the photocathode via the photoelectric effect; the bunch charge, the energy and the transverse properties of the electron beam are different from the dark current. Thus, the behavier of the electron beam dependence on the solenoid focusing condition is different. The electron beam images on the screen for the solenoid magnetic fields of 0-297 mT are shown in Fig. 4.25.

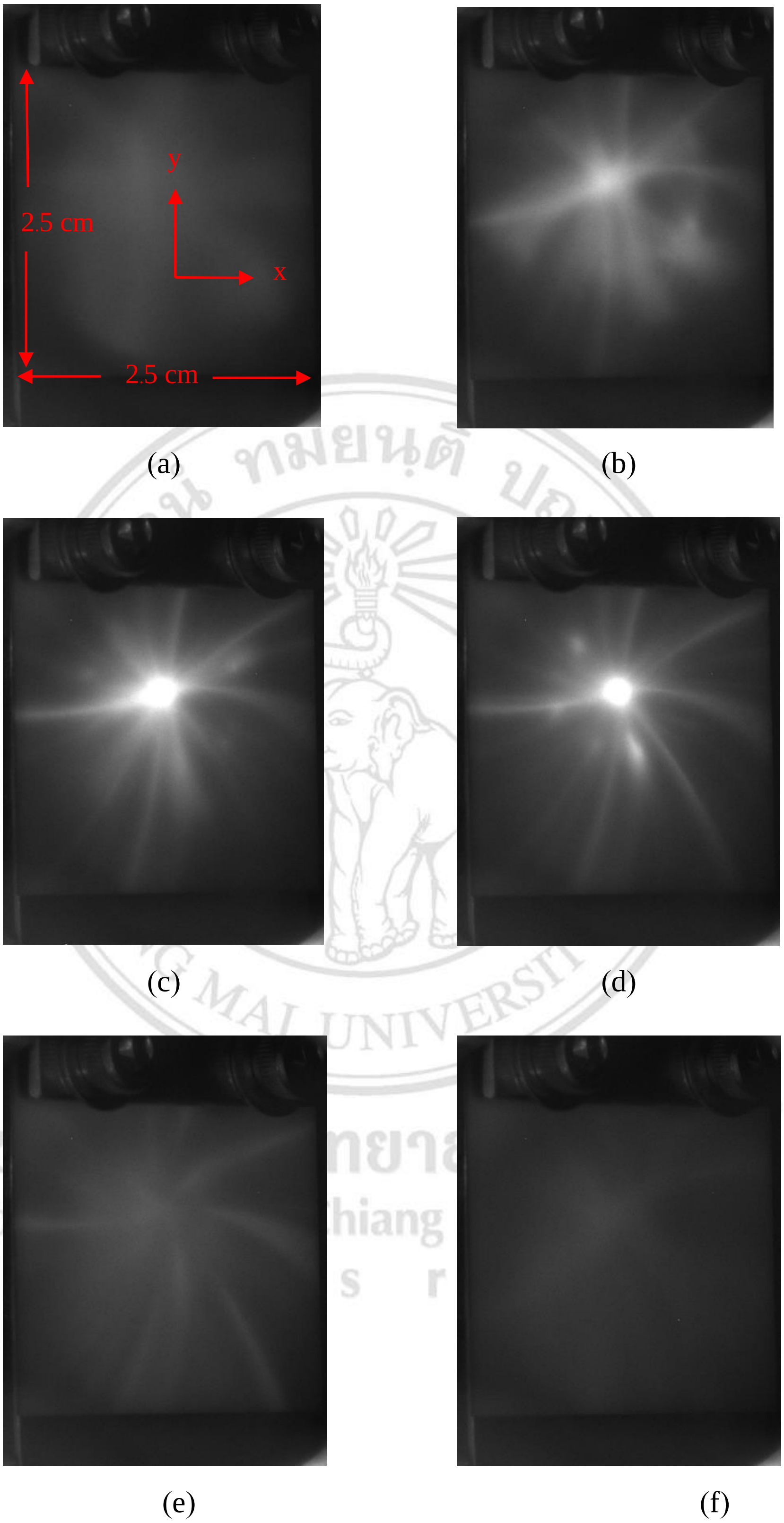

Figure 4.24: The dark current images on the screen for the solenoid magnetic fields of (a) 0 mT, (b) 104 mT, (c) 156 mT, (d) 193 mT, (e) 222 mT and (f) 297 mT.

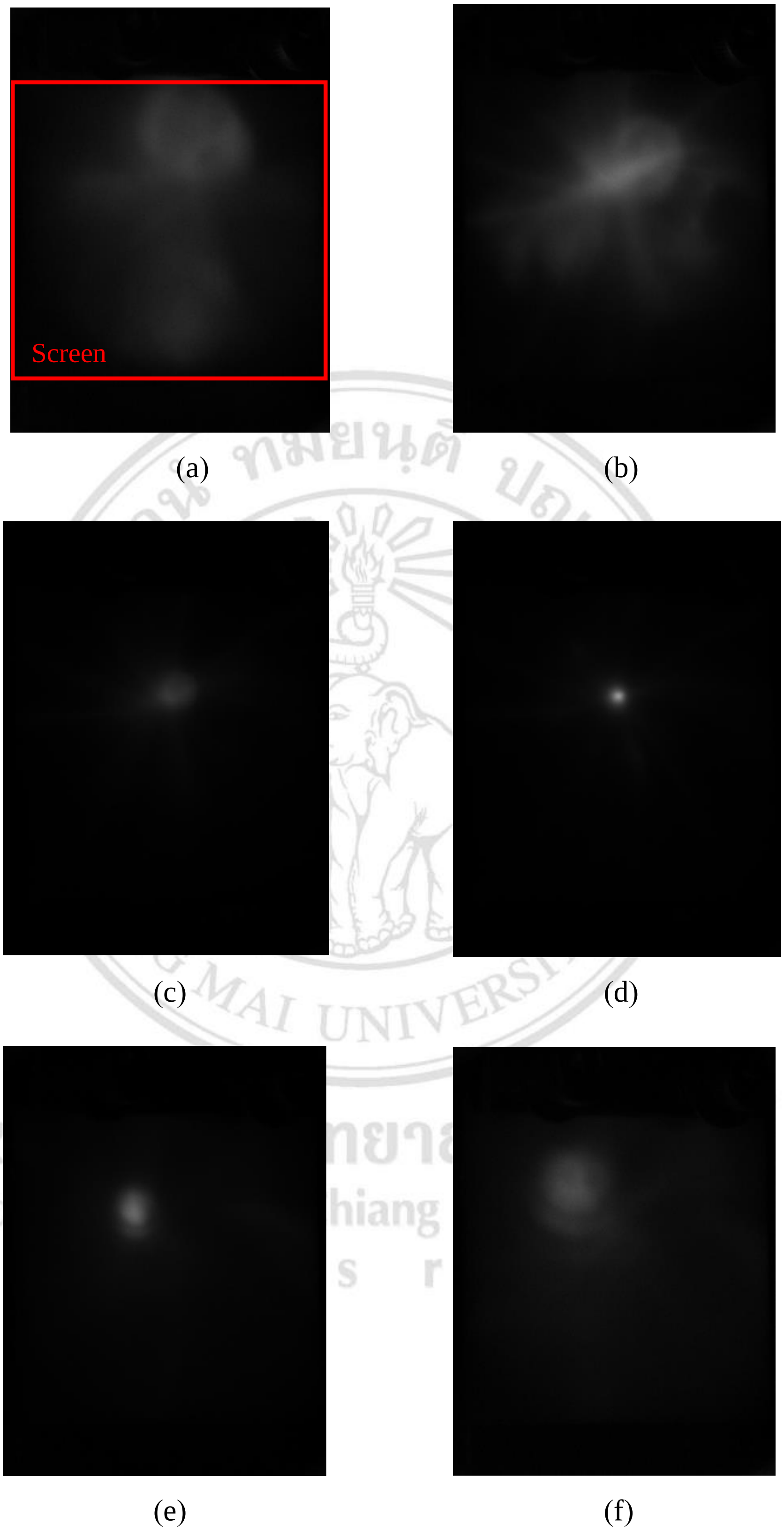

Figure 4.25: Electron beam images on the screen for the solenoid magnetic fields of (a) 0 mT, (b) 104 mT, (c) 163 mT, (d) 193 mT, (e) 252 mT and (f) 297 mT.

The study results show that the electron beam cannot be performed without the solenoid magnetic focusing. An optimal transverse beam size at this screen occurs when using the solenoid magnetic field of around 192.8 mT. The optimal transverse size in the x-axis and the y-axis are 0.94 and 0.89 mm, respectively. The transverse beam size increases when the solenoid magnetic field is larger than 252 mT. The beam center changes its position when the solenoid magnetic focusing changes. The center of the dark current is used as a reference point for studying the electron beam center dependence on the solenoid magnetic field. The measured result of the beam center dependence on the solenoid magnetic field at z = 78 cm is shown in Fig. 4.26.

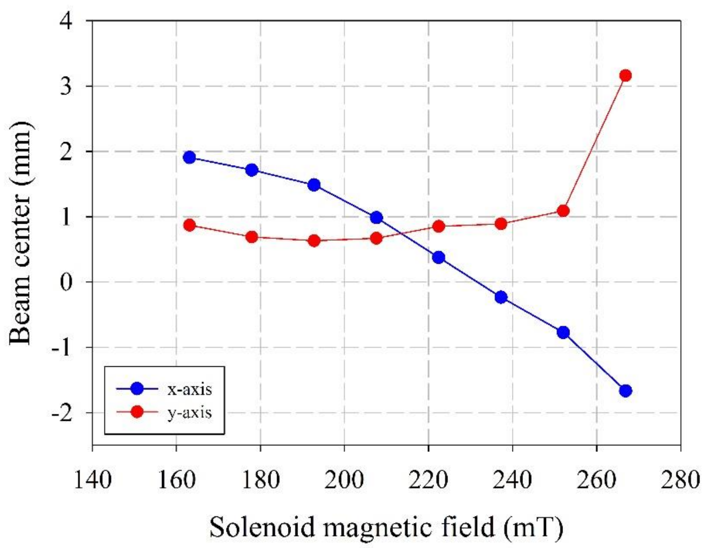

Figure 4.26: Measured result of the beam center dependence on the solenoid magnetic field.

The results in Fig. 4.26 show that the beam center in the x-axis shifts from x = +1.9 mm to x = -1.6 mm and the beam center in y-axis varies in the range of y = +0.6 mm to y = +3.1 mm for the solenoid magnetic field range of 163 - 266 mT. Possible reasons of shifting in the beam position are the electrons are not generated at the photocathode center and the solenoid magnet was not perfectly alignment. Thus, the electron beam did not travel through magnetic field at the solenoid magnet center. Since the electron beam feels the unbalance solenoid magnetic force, the beam position changes when the solenoid magnetic field changes.

In this thesis, the PARMELA simulation program was used to study the dependence of electron beam center shifted position on the injected laser position and the solenoid magnetic field. The simulated parameters are shown in Table 4.2. Relationships between the electron beam center and the solenoid magnetic field at z = 78 cm downstream the photocathode when the injected laser positions shift in the +x-axis and +y-axis are shown in Fig. 4.27. An example of the cross-sectional area of the photocathode and the electrons, which are generated with +0.1 cm-shifted drive laser, is shown in Fig. 4.28.

Table 4.2: Simulated parameters used in PARMELA simulations in section 4.4.

Parameter	Value
Resonant frequency	2,856 MHz
Laser spot size at FWHM	1.378 mm
Laser pulse length at FWHM	8 ps
Accelerating gradient E_1 and E_2	52 MV/m
RF phase	40 degree
Electron bunch charge	50 pC
Solenoid magnetic field	0 – 300 mT

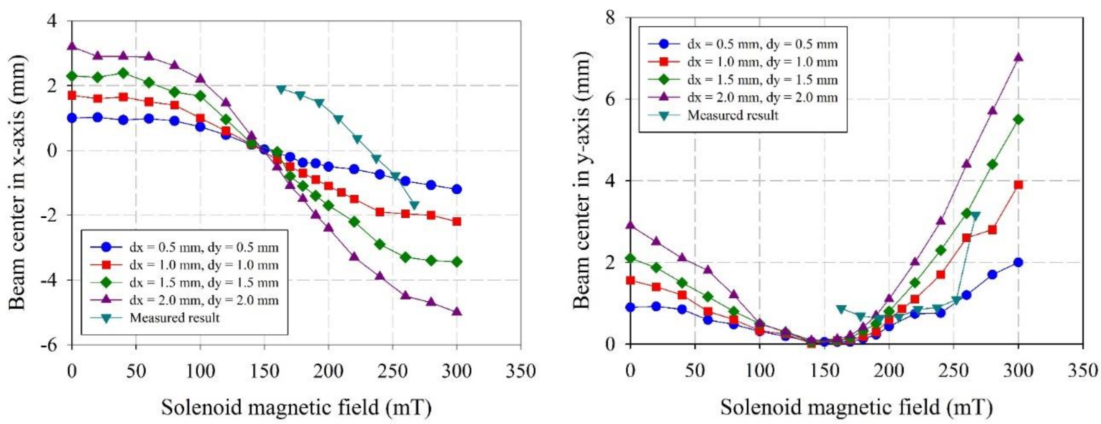

(a) (b)

Figure 4.27: Dependence of simulated electron beam center in (a) x-axis and (b) y-axis on the solenoid magnetic field and the shifted laser injection positions on the photocathode.

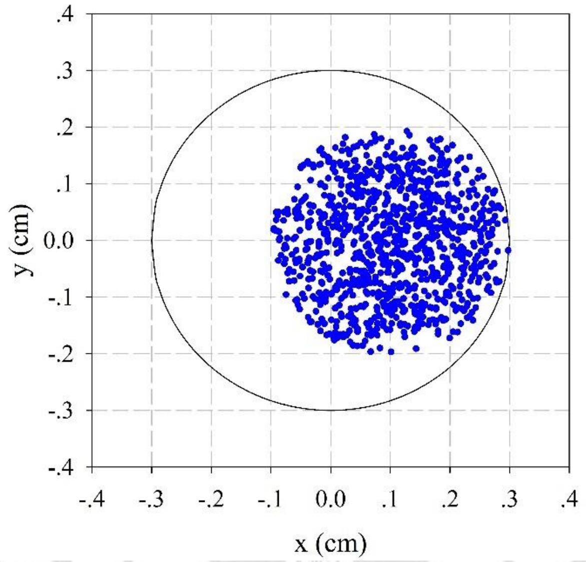

Figure 4.28: Cross-sectional area of the photocathode and the electrons, which are generated by the +0.1 cm-shifted drive laser.

As shown in Fig. 4.27, the beam center at the photocathode shift in +x and +y directions. The electrons, which are generated from the shifted-position photocathode drive laser, are deflected by the magnetic field, which is not zero when z ≠ 0. This leads the electrons to have large transvers and angular displacement. When the solenoid magnetic field is used to control the electron beam transverse properties, the solenoid magnetic force acts on the beam in both x-axis and y-axis. The shifted electron beam feels unbalance force and its traveling direction is bent while it trvels through the solenoid magnetic field.